SUPPORTING INFORMATION

Turn Plasticity Distinguishes Different Modes of Amyloid-β Aggregation

Nasrollah Rezaei-Ghaleh, Mehriar Amininasab, Karin Giller, Sathish Kumar, Anne Stündl, Anja Schneider, Stefan Becker, Jochen Walter, and Markus Zweckstetter

Supplementary Methods

Transmission Electron Microscopy. Wild-type and S26D-Aβ40 samples of 0.1 mg/mL concentration in HEPES buffer (25 mM, pH 7.4, 50 mM NaCl) were incubated at 37 °C with gentle stirring. After 3 and 48 hours of incubation, samples were diluted, deposited onto carbon-coated copper mesh grids and negatively stained with 2 % (w/v) uranyl acetate. The excess stain was washed away, and the sample grids were allowed to air-dry. The samples were then viewed with a 120-kV transmission electron microscope.

Cell viability assay. Primary cortical neurons were prepared from E16 NMRI mouse embryos and cultured on poly-lysine-coated 48-well dishes in serum-free MEM supplemented with B27 (Invitrogen). Cell viability was quantified using the 3-(4,5-dimethylthiazol-2-yl)-2,5-diphenyltetrazolium bromide (MTT, Sigma-Aldrich) reduction assay. Solutions of synthetic Aβ (100 µM) in PBS were incubated for 48 hours at 37 °C under gentle stirring, then primary cortical neuronal cells (DIV 8) were treated with peptide solutions (at final concentration of 10 µM) for 48 hours. For viability assay, cells were incubated for 1 hour at 37°C in medium containing 0.5 mg/mL MTT. Cells were solubilized with dimethyl sulfoxide (DMSO, AppliChem) for 20 minutes and absorbance was measured at 570 nm on a plate reader (Omega Fluostar, BMG Labtech). Measurements were performed in duplicates.

Supplementary Figures

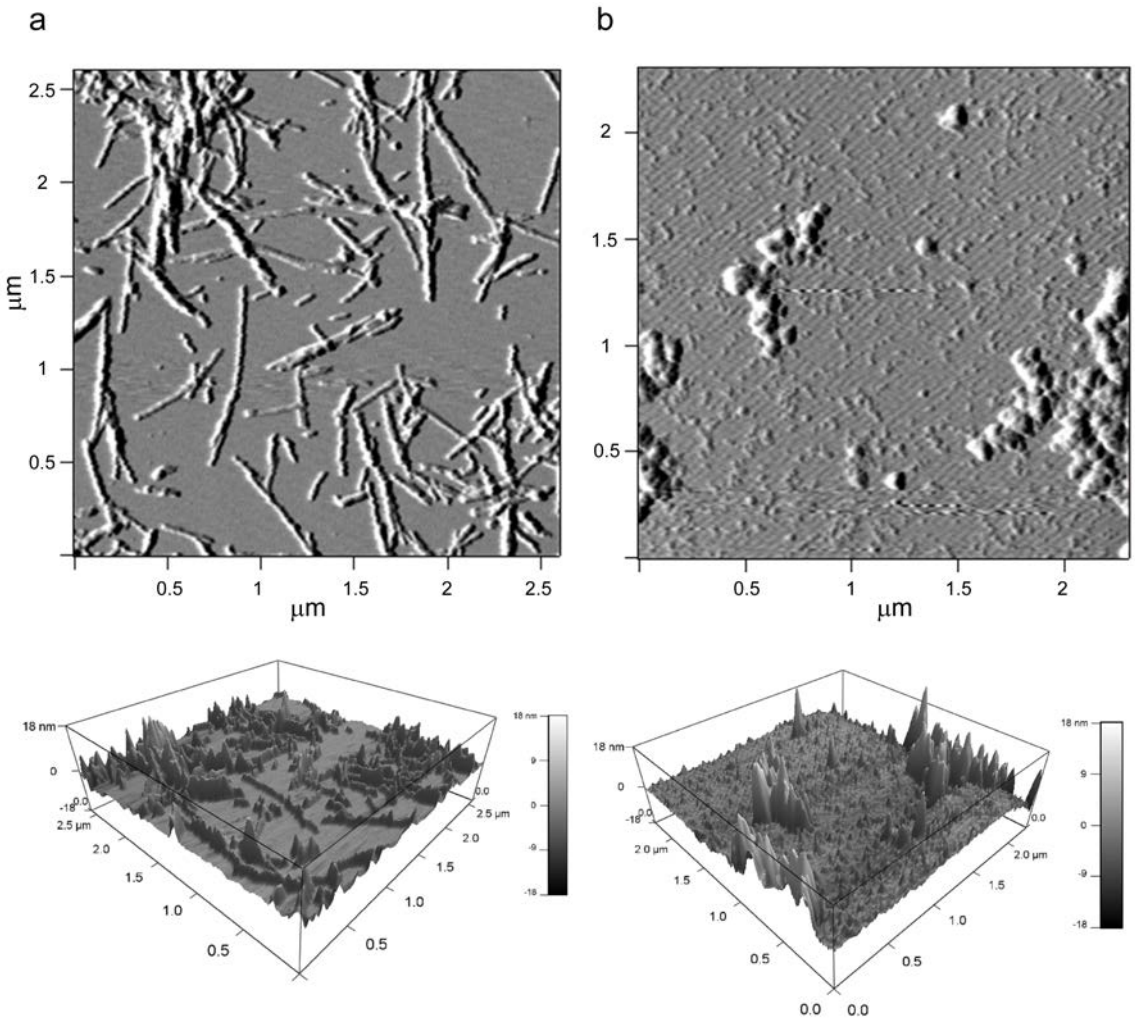

Figure S1. Atomic Force Microscopy (AFM) images of Aβ40 after 2 days of aggregation, along with the 3D representation of surface topography. The *wt*-Aβ40 is aggregated into fibrils (a), while pS26-Aβ40 forms non-fibrillar assemblies of up to 30 nm in diameter (b).

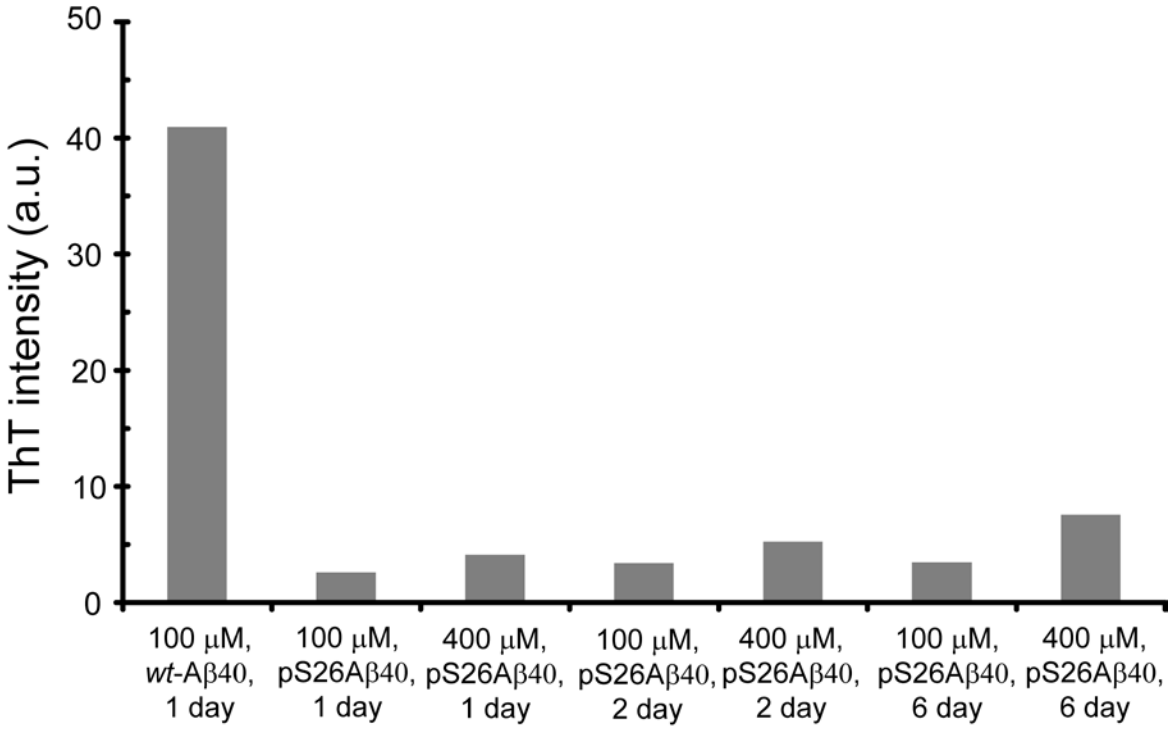

Figure S2. Influence of peptide concentration and incubation times on formation of ThT-reactive aggregates by pS26-Aβ40. Even at a peptide concentration of 400 μM only a small increase in ThT fluorescence was observed after 6 days of incubation.

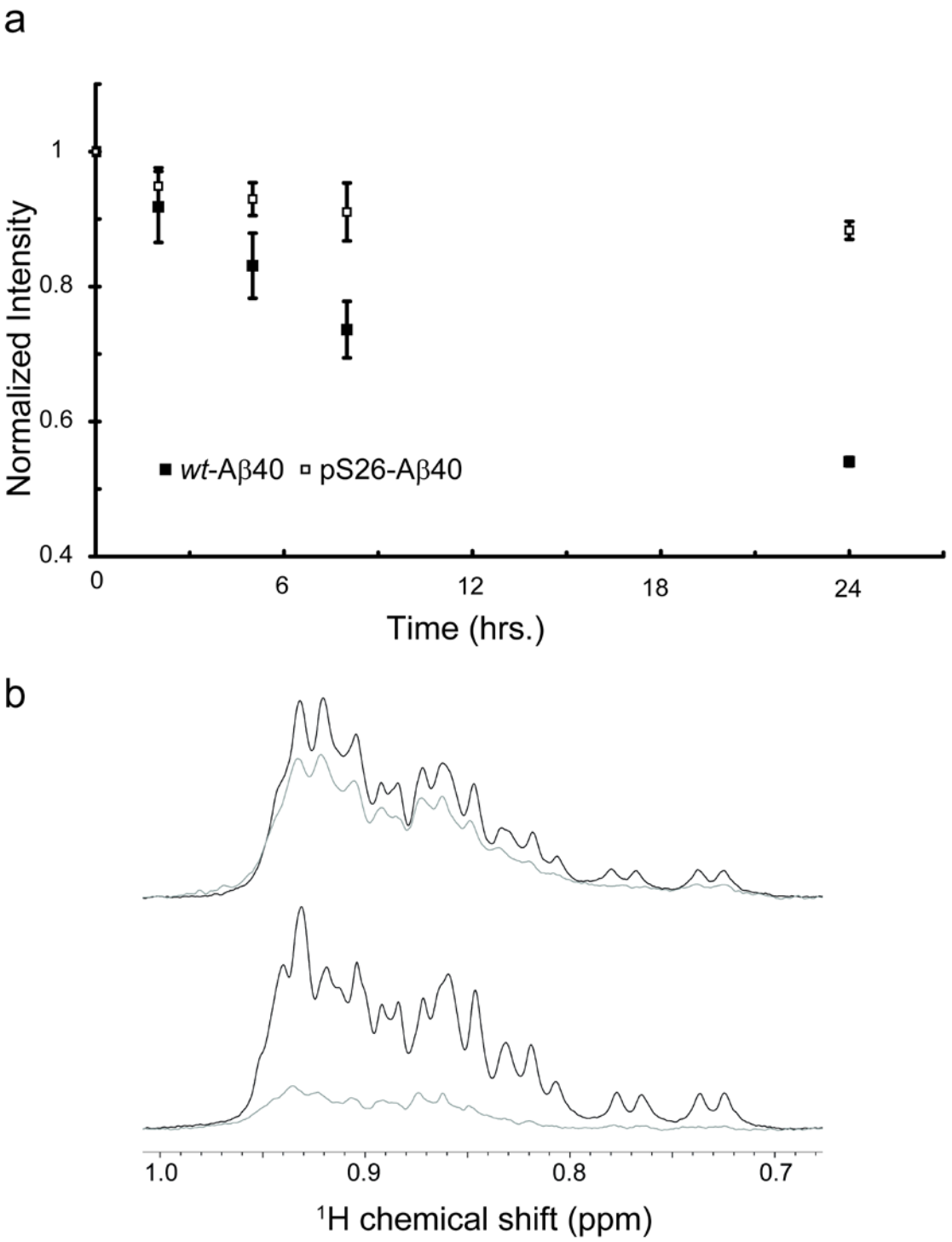

Figure S3. Monomer consumption assay using 1D ^{1}H NMR spectroscopy. (a) Over a 24-hour period of aggregation in the NMR tube, nearly half of *wt*-Aβ40 (filled symbols) and ~10% pS26-Aβ40 (open symbols) monomers were converted into NMR invisible aggregates. (b) 1D ^{1}H spectra of *wt*- (bottom) and pS26-Aβ40 (top) in the methyl region, before (black) and after (gray) 3-days incubation in a more aggregation prone condition (as used in CD experiment, Figure 2c). The monomer loss increased to 80% and 20%, for *wt*- and pS26-Aβ40 respectively.

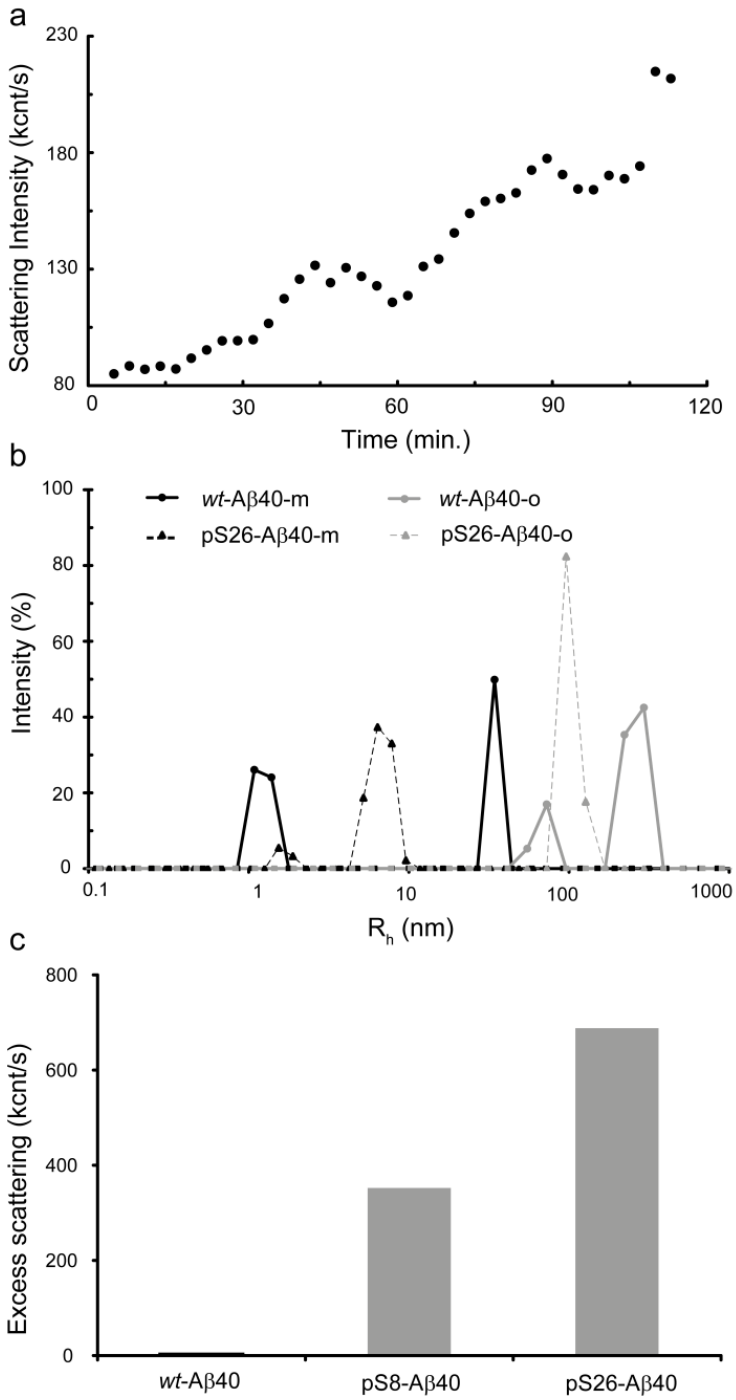

Figure S4. Dynamic light scattering of soluble Aβ40 aggregates. (a) Changes in light scattering intensity of pS26-Aβ40 during the first two hours of incubation in aggregation-promoting condition. (b) Size distribution of Aβ40 before (m, "monomeric") and after (o, "oligomeric") incubation in aggregation-promoting condition. The pS26-Aβ40 sample contained monomers (R_h of ~ 1-2 nm) and small oligomers (R_h of ~ 7-9 nm) before aggregation, which upon aggregation were converted to larger oligomers (R_h of ~ 100 nm). (c) Scattering intensities of aggregated Aβ solutions after centrifugation to remove any insoluble aggregates.

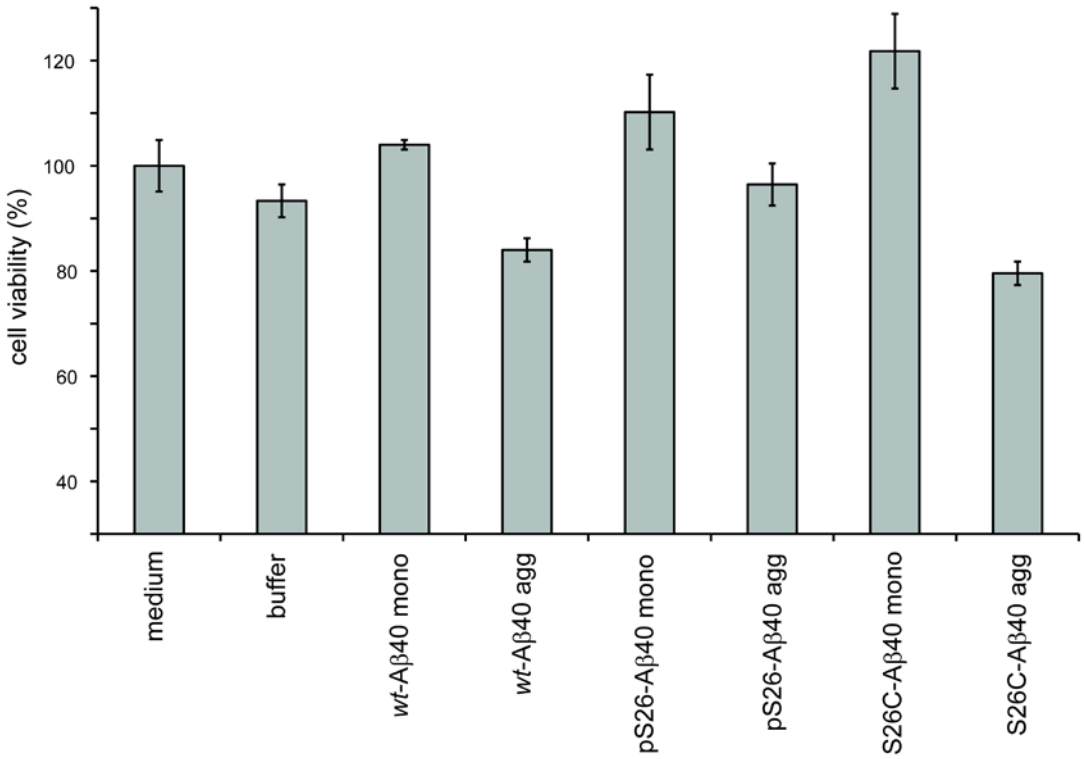

Figure S5. Cell viability assay of Aβ aggregates in primary cortical neurons. Following a 48-hour treatment of neurons (DIV8) with the indicated peptide preparations, the neuronal viability was determined by MTT assay. Results are shown as means±SEM (n=2). Compared to the control (medium, buffer), the aggregated *wt*- and S26C-Aβ40 decreased the cell viability, but pS26-Aβ40 did not cause a significant reduction in cell viability.

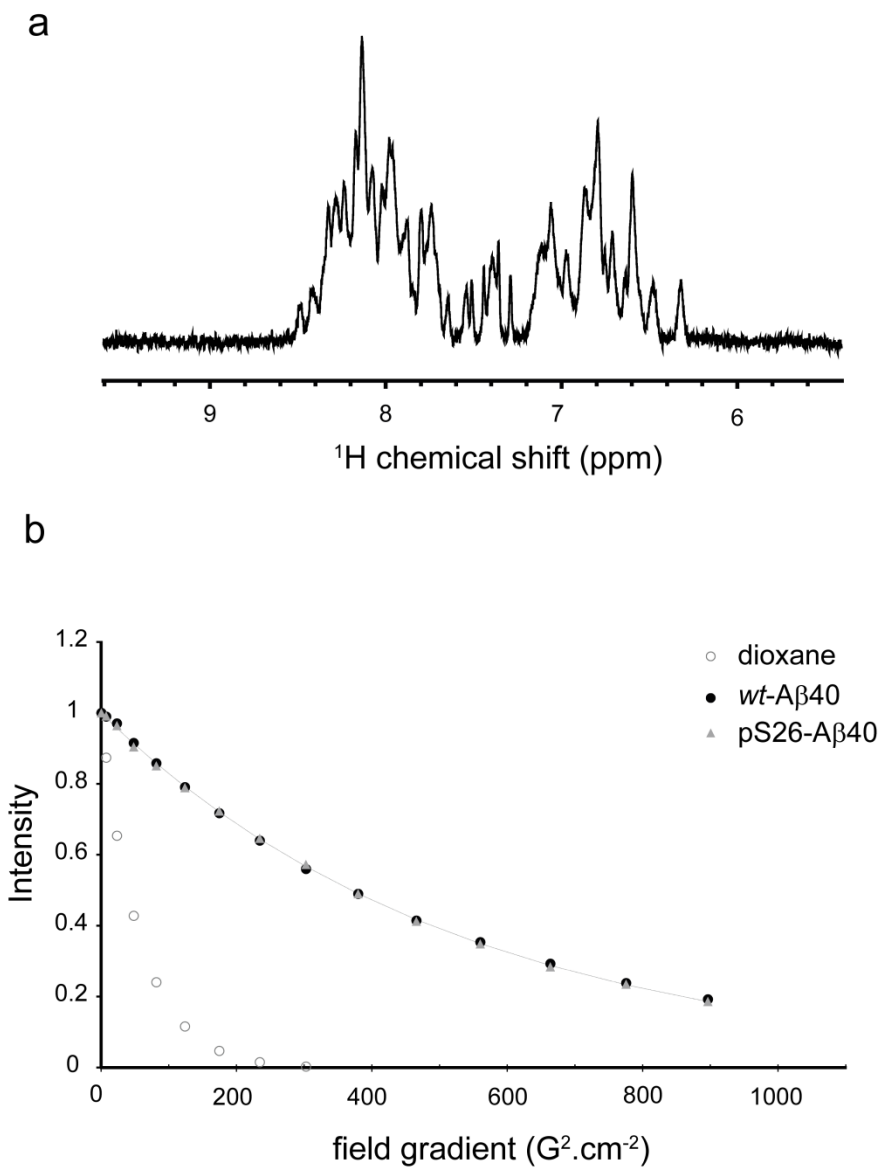

Figure S6. Aβ40 is intrinsically disordered in solution. (a) 1D ^{1}H NMR spectrum of Aβ40. (b) PFG-NMR based diffusion measurements of *wt*- and pS26-Aβ40. The obtained hydrodynamic radius for Aβ40 (~ 1.6 nm) is consistent with its disordered nature.

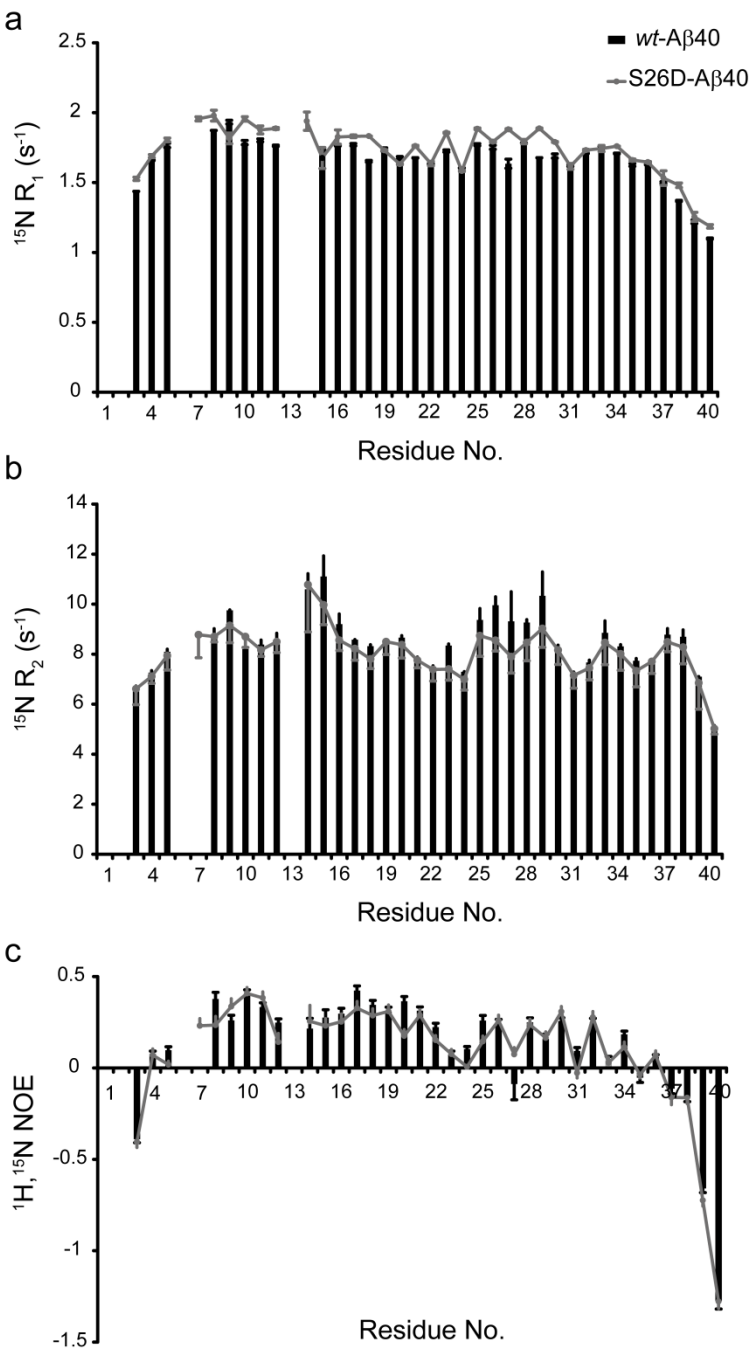

Figure S7. ^{15}N spin relaxation rates in *wt*- (black) and S26D-Aβ40 (gray). (a) R_1 longitudinal relaxation rates. (b) R_2 transverse relaxation rates. (c) ^{1}H,^{15}N steady-state heteronuclear NOE.

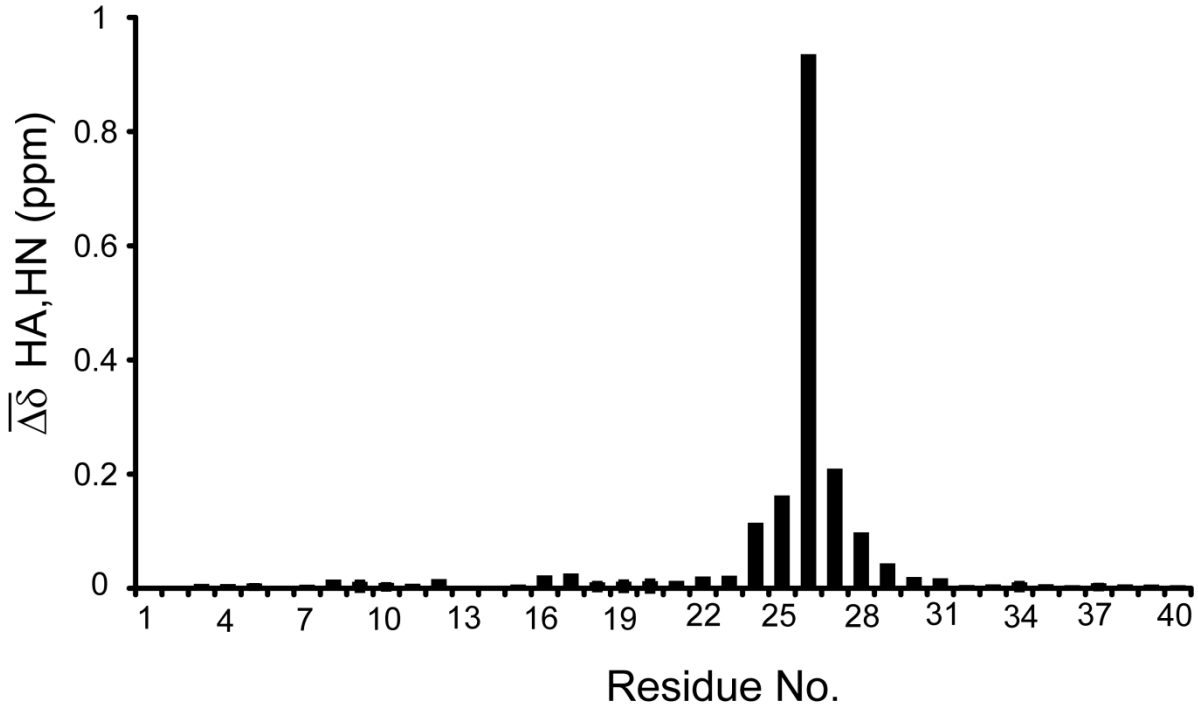

Figure S8. Combined HA and HN chemical shift difference ($\sqrt{(\Delta\delta HA)^2 + (\Delta\delta HN)^2}$) between *wt*- and pS26-Aβ40 as a function of residue number. Only residues 24-29 close to the site of modification are significantly affected.

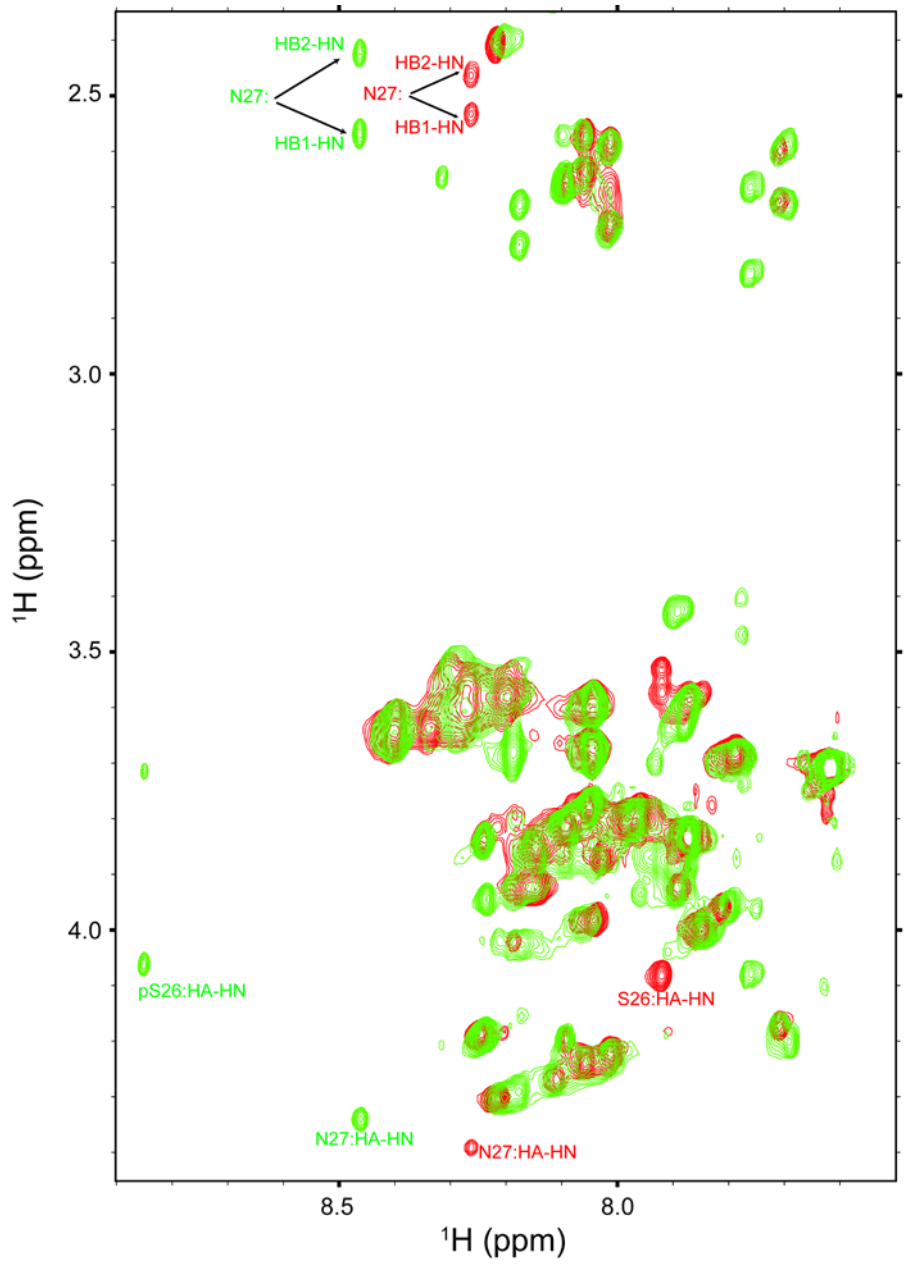

Figure S9. Selected region of 2D ^{1}H,^{1}H TOCSY spectra of *wt*- (red) and pS26-Aβ40 (green), highlighting the correlation peaks between amide and either α- or β-protons of the modified residue, S26, and the following residue, N27. Note that the dispersion between the two HB resonances of the N27 side chain was increased after S26 phosphorylation.

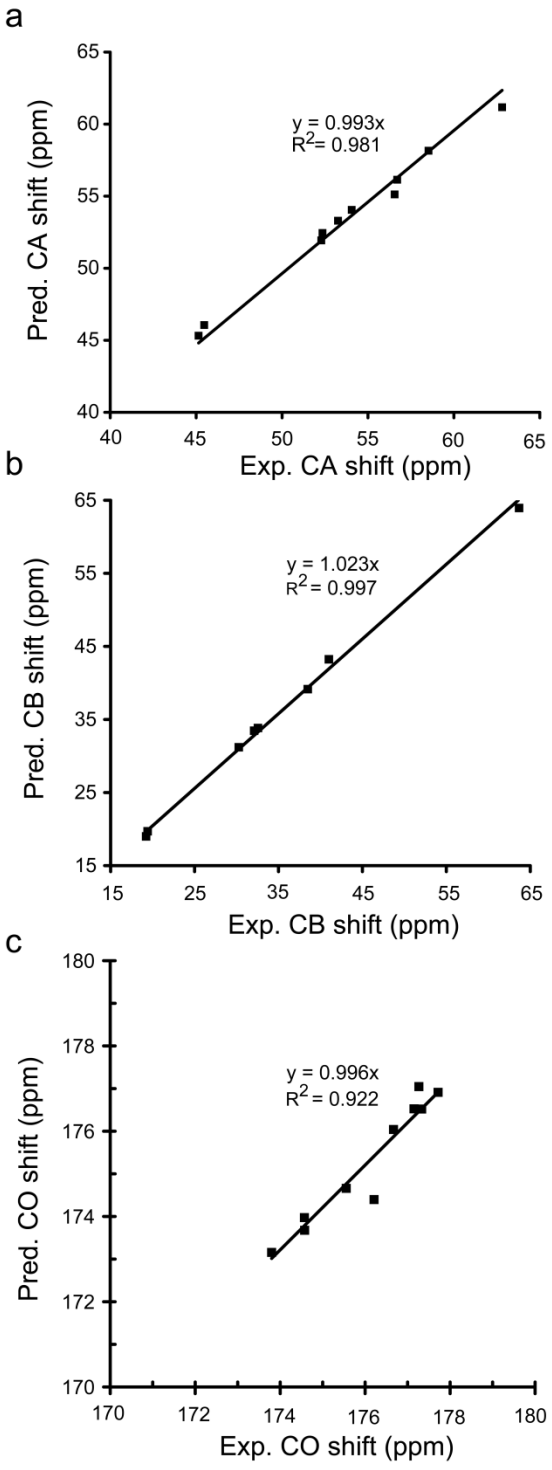

Figure S10. Correlation between experimentally observed ^{13}CA (a), ^{13}CB (b) and ^{13}CO (c) NMR chemical shifts of *wt*-Aβ40 with those predicted from the MD ensemble of *wt*-Aβ(21-30).

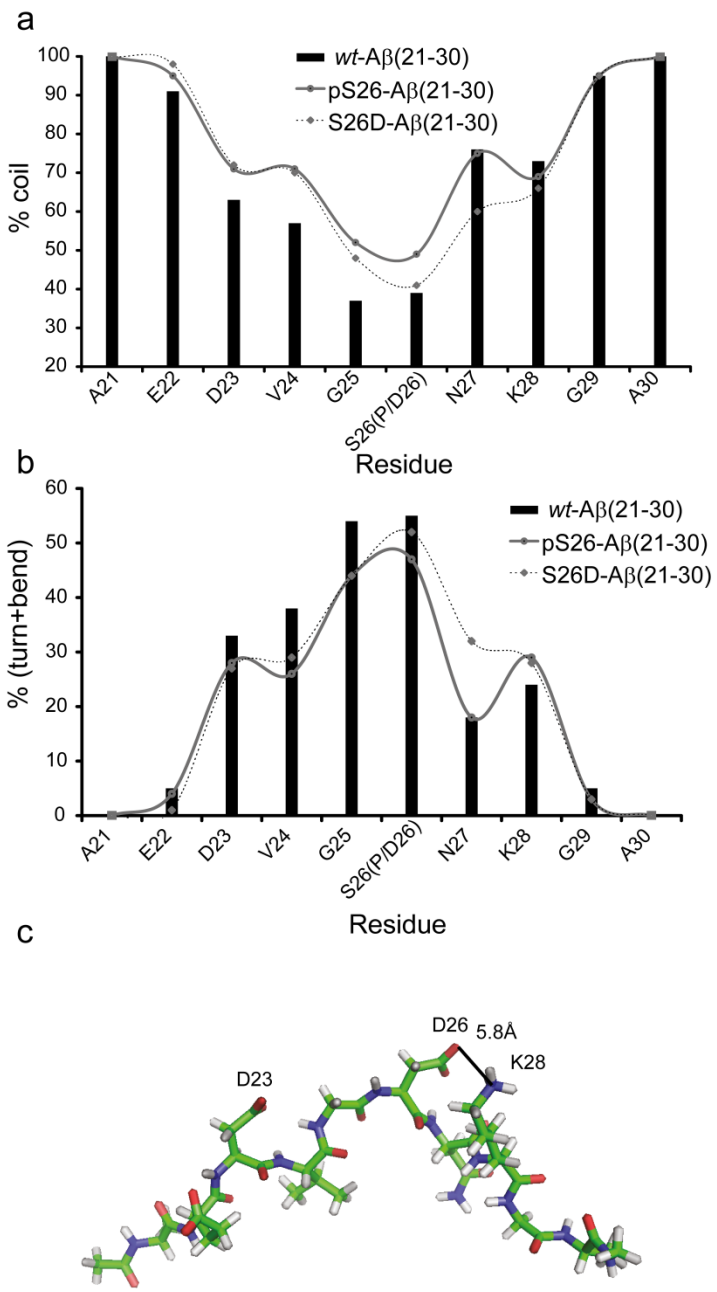

Figure S11. Structural propensities observed in MD simulations of *wt*- (gray), S26D (dashed) and pS26-Aβ(21-30) (black). (a) Percentage of coil conformations. (b) Percentage of turn or bend conformations. (c) Representative structure of the highest populated cluster of S26D-Aβ(21-30). The side-chain of K28 is located in close proximity to the oppositely-charged side-chain of D26.

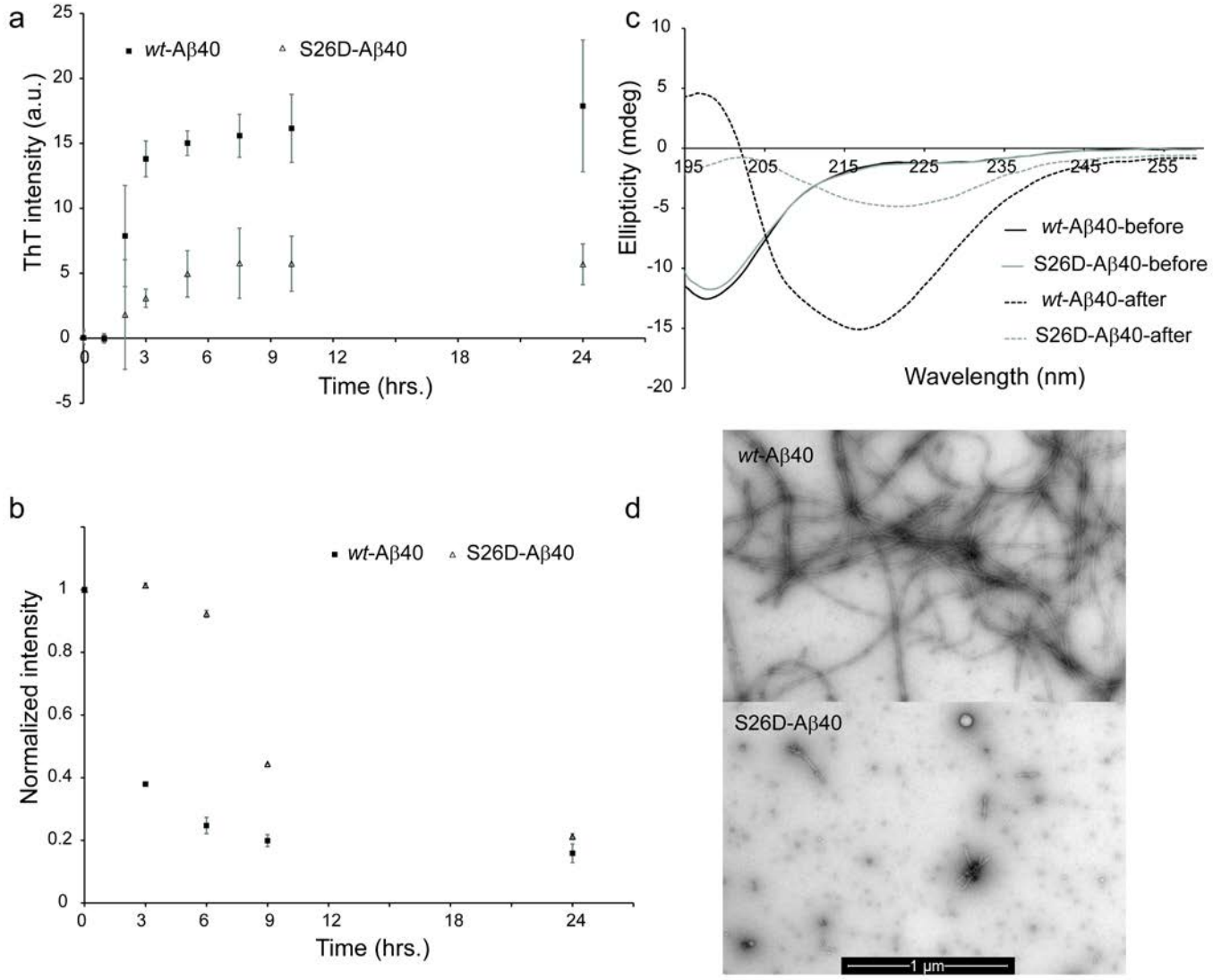

Figure S12. The phosphomimetic S26D mutation reduces the rate and amount of β-sheet-rich fibrillar aggregation of Aβ40. (a) Evolution of ThT fluorescence emission intensity over the course of incubation of *wt*- and S26D-Aβ40 in an aggregation promoting condition. (b) Monomer consumption assay using 1D ^{1}H NMR spectroscopy. Note that in the case of S26D-Aβ40, a significant loss in monomer concentration occurs only after 6 hours of incubation. (c) Far-UV CD spectra of *wt*- and S26D-Aβ40, before and after 48 hours of incubation in an aggregation-promoting condition. Upon aggregation, *wt*- and to a less degree, S26D-Aβ40 are converted from mainly random coil states to extended β-sheets. (d) Electron micrographs of *wt*- and S26D-Aβ40 incubated for 3 hours in an aggregation promoting condition. The *wt*-Aβ40 forms many long twisted fibrils, but S26D-Aβ40 forms only oligomers and few short fibrils.

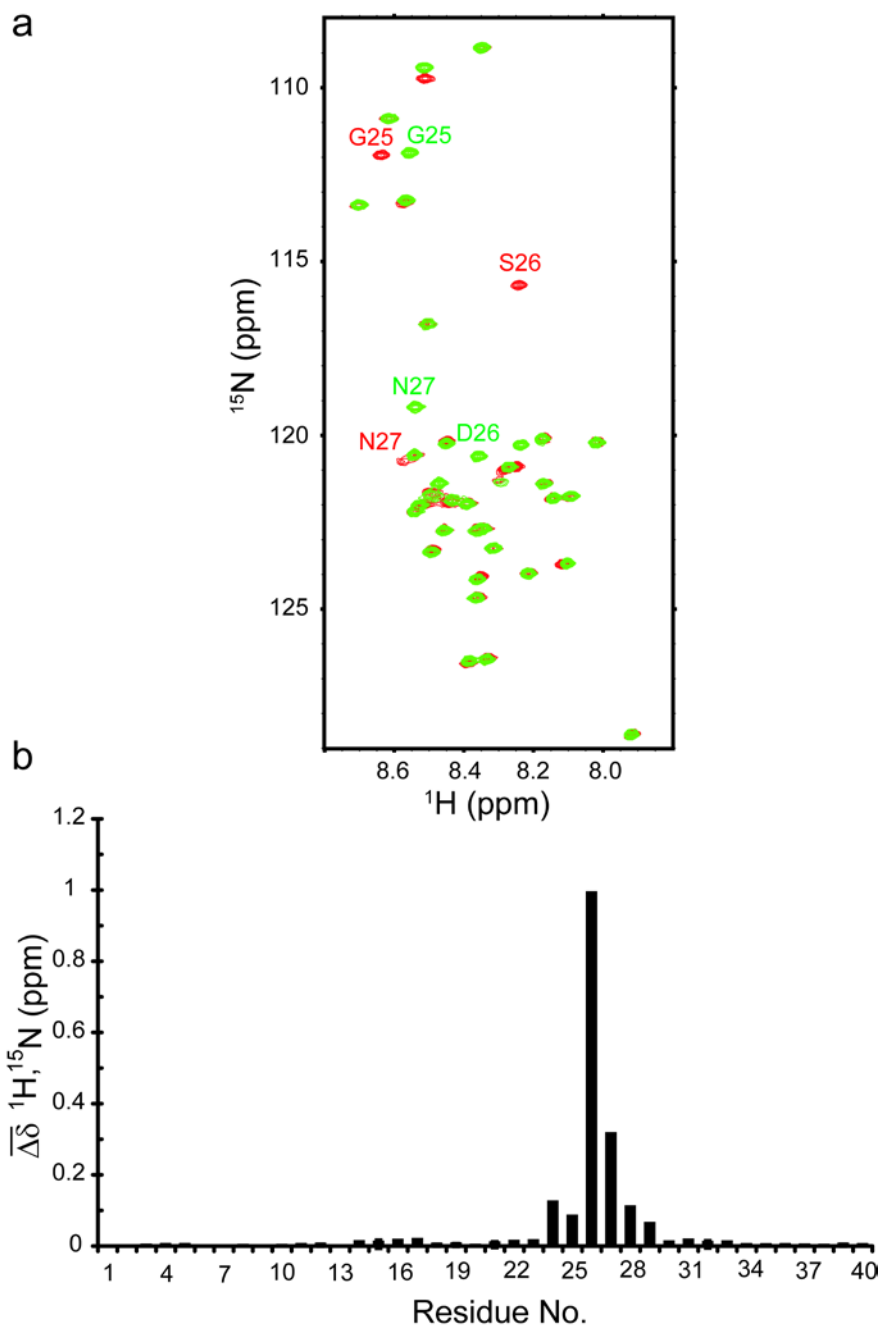

Figure S13. (a) The overlay of ^{1}H,^{15}N HSQC spectra of *wt*-Aβ40 (red) and the phosphomimetic mutant S26D-Aβ40 (green). (b) Combined ^{1}H,^{15}N chemical shift difference ($\sqrt{(0.2\Delta\delta N)^2 + (\Delta\delta H)^2}$) between *wt*- and S26D-Aβ40. Only residues 24-29 next to the site of mutation were significantly affected.

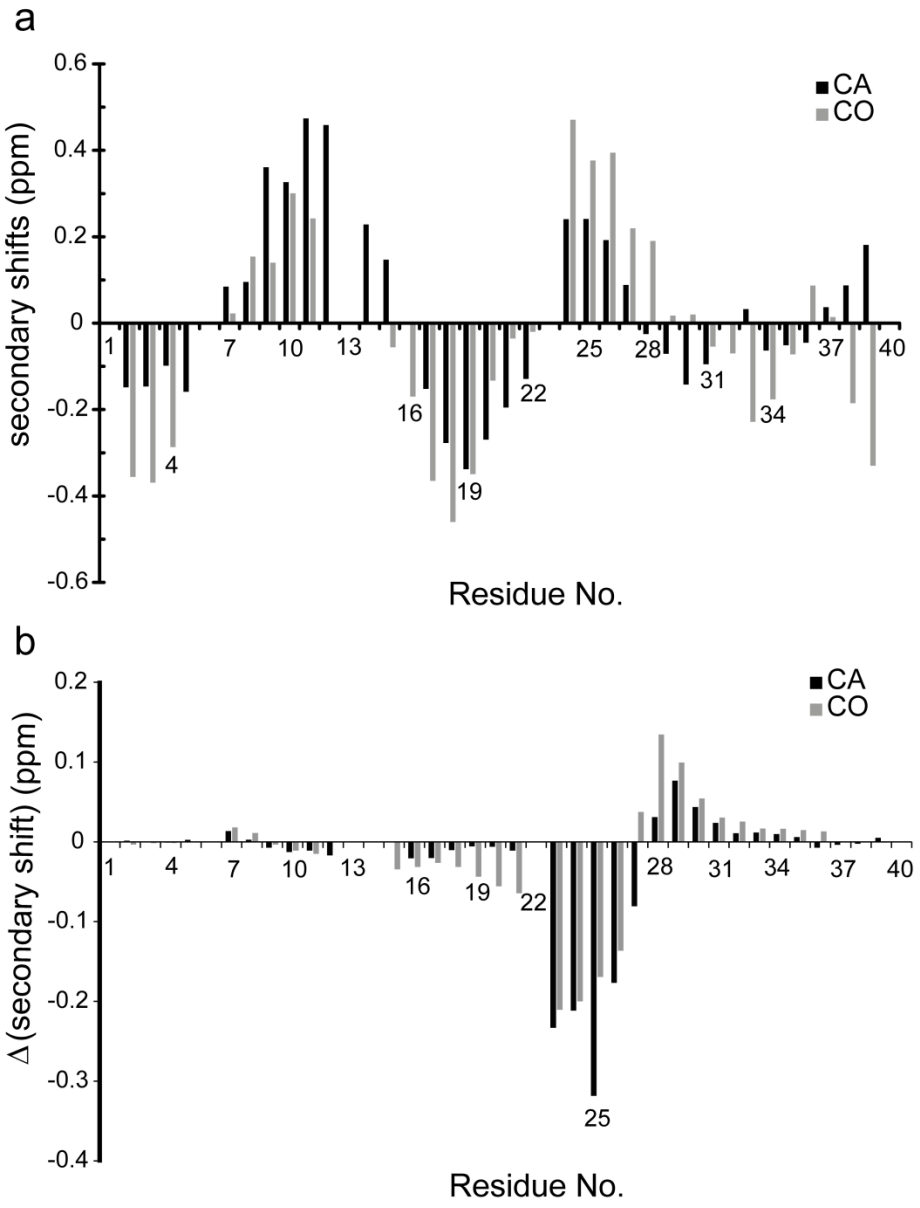

Figure S14. Secondary structure propensities of *wt*- and S26D-Aβ40. (a) Residue-specific differences between experimental CA and CO NMR chemical shifts and predicted random coil values (so-called secondary shifts, ΔCA and ΔCO) of *wt*-Aβ40. (b) Changes in secondary CA (Δ (ΔCA)) and CO chemical shifts (Δ (ΔCO)) upon S26D mutation.

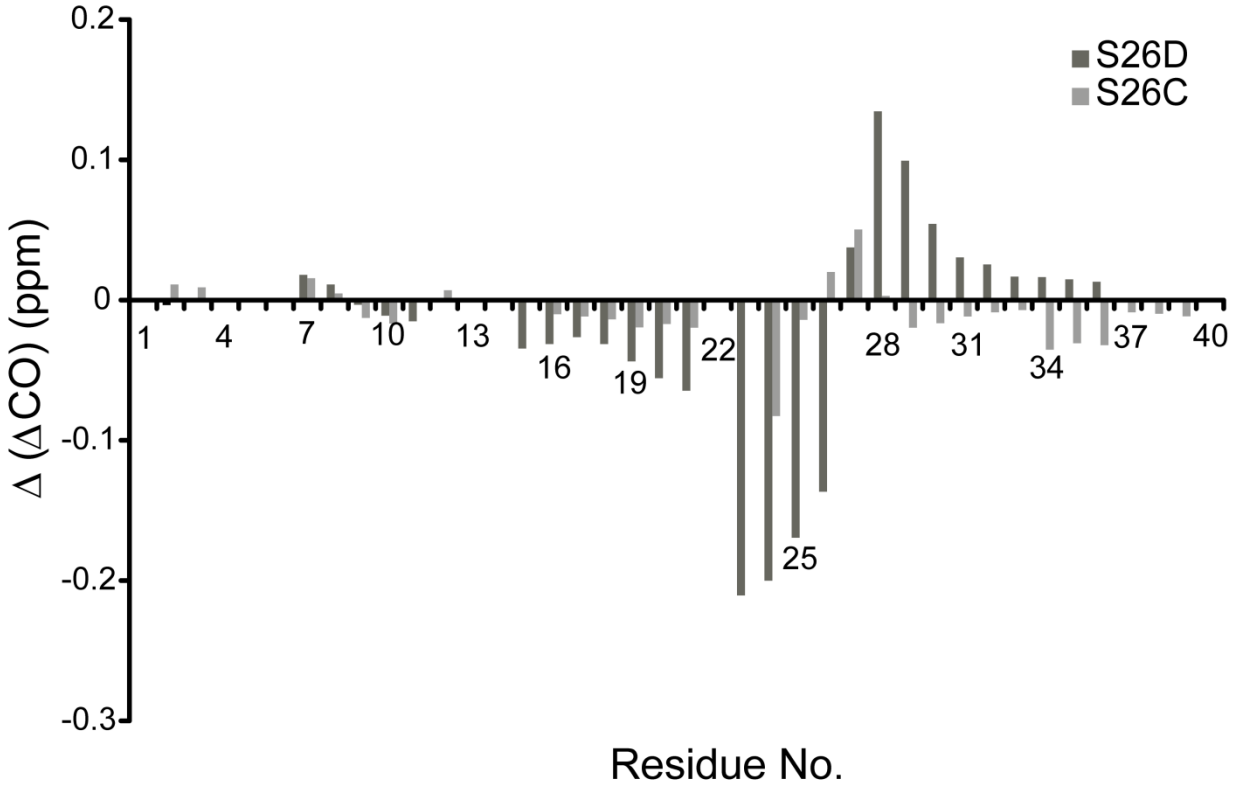

Figure S15. Comparison between the effects of S26D (dark gray) and S26C (light gray) mutations on secondary CO shifts (Δ (ΔCO)) of Aβ40. S26C-Aβ40 was kept in reducing condition (1 mM TCEP).

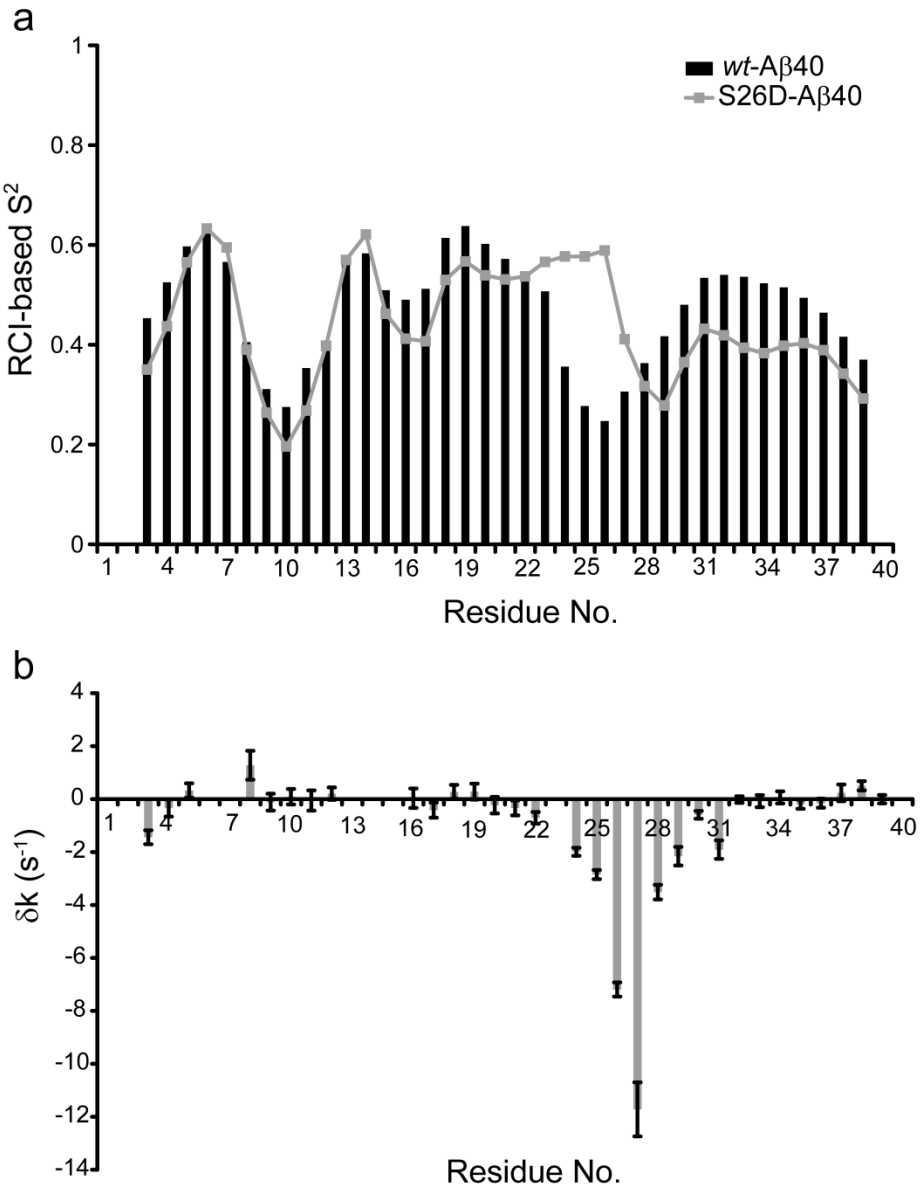

Figure S16. Residue-specific changes in conformational dynamics of Aβ40 upon S26D mutation. (a) Random coil index-based squared order parameters (S^2) of *wt*- (black) and S26D-Aβ40 (gray), calculated from CA, CB, CO, N, HN and HA chemical shifts. An increase in order parameter of residues 23-27 indicates higher rigidity of this region in S26D-Aβ40. (b) Changes in water-amide proton exchange rates upon S26D mutation.

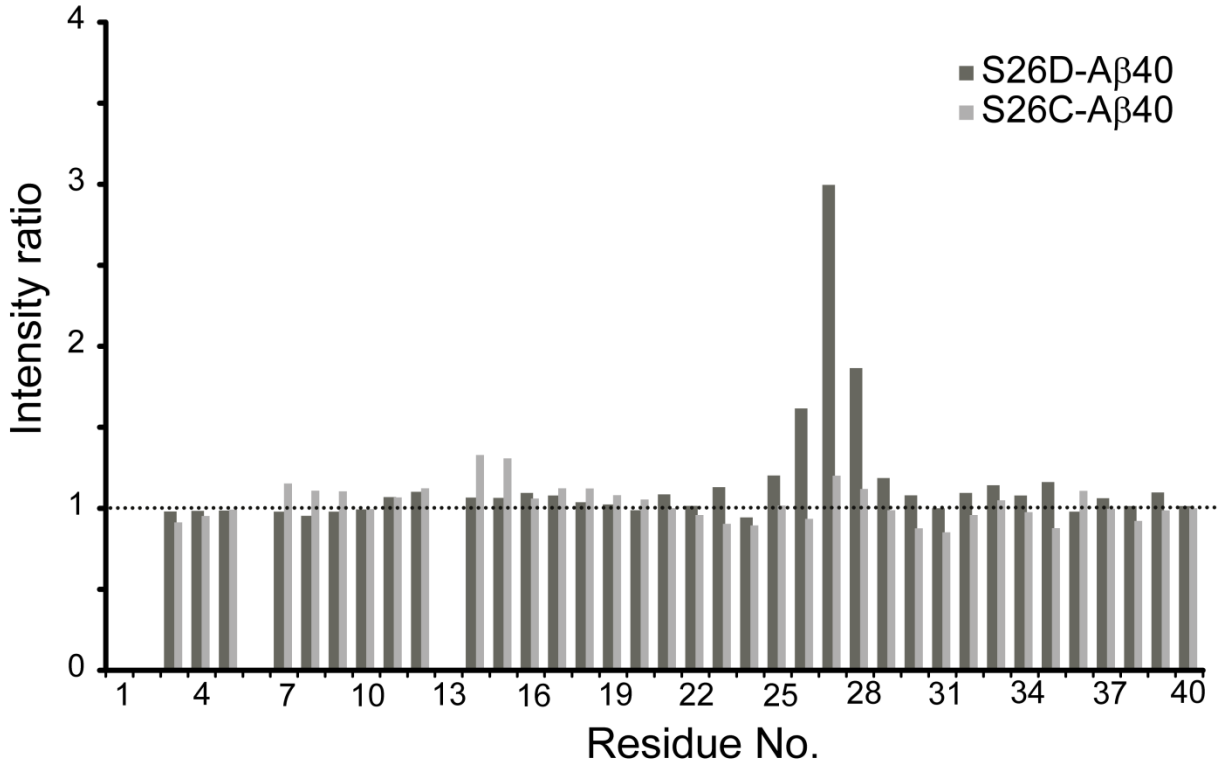

Figure S17. Intensities of cross peaks observed in 2D $^{1}H,^{15}N$ HSQC spectra of S26D- (dark gray) and S26C-Aβ40 (light gray) normalized by cross peak intensities of *wt*-Aβ40. S26C-Aβ40 was measured in reducing condition (1 mM TCEP). In S26D-Aβ40, residues S26, N27 and K28 gain in intensity, supporting their decreased conformational mobility on the micro-to-millisecond time scale.